ACS APPLIED MATERIALS & INTERFACES

www.acsami.org

Research Article

Relationship between Desalination Performance of Graphene Oxide Membranes and Edge Functional Groups

Ruosang Qiu, Jie Xiao, Xiao Dong Chen, Cordelia Selomulya, Xiwang Zhang, and Meng Wai Woo*

Cite This: *ACS Appl. Mater. Interfaces* 2020, 12, 4769–4776

Read Online

ACCESS | Metrics & More | Article Recommendations | Supporting Information

ABSTRACT: High desalination efficiency in principle could be achieved by layer-by-layer graphene oxide (GO) membranes, which benefits from their entrance-functionalized channels assembled by edge-functionalized GO nanosheets. The effects of these edge functional groups on desalination, however, are not fully understood yet. To study the isolated influence of three typical edge functional groups, namely, carboxyl (-COOH), hydroxyl (-OH), and hydrogen (-H), molecular dynamics simulation was used in this work. The results revealed that the edge volumetric blockage effect, resulting in ion permeability at G-H > G-OH > G-COOH membranes, was the dominant mechanistic effect inside the GO membranes with 7 Å interlayer channels. The OH edge has the same effect as the H edge in NaCl/water selectivity because of a unique "ion pulling" effect. Moreover, the OH and H edge-functionalized membranes with 7 Å interlayer channels showed preferential Na^+ and Cl^- rejections, respectively. This kind of preference leads to a cycle of charging and neutralization in the penetrant reservoir throughout the filtration process. The results from this work suggested that it would be strategic to keep the COOH and H edge functional groups, to maintain the size of interlayer channels in order to stimulate the effects of edge functional groups, and to increase the membrane porosity for designing higher desalination efficiency GO membranes.

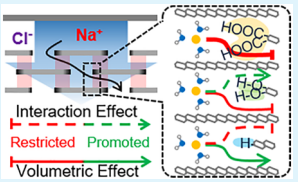

KEYWORDS: *graphene oxide membranes, edge functionalization, COOH edge, OH edge, H edge, desalination performance, preferential ion rejection*

INTRODUCTION

Membrane-based filtration technology has seen increasing growth to desalinate saline water and reduce freshwater shortage because of its low energy consumption and operation cost but high desalination efficiency.[1−3] Commercial desalination membranes are currently made of polymers,[4−6] whose structures are hard to be controlled and may be easily destroyed for their low chemical tolerance. The two-dimensional (2D) graphene oxide (GO)-based membrane, compared with polymeric membranes, has higher chemical and physical stability.[7] 2D GO nanosheets, which play a similar role as the cross-linked polymer inside the membrane, can naturally be assembled into a well-packed layer-by-layer structure. This unique structure inside the membranes provides transmembrane molecules with winding channels in a controlled and uniform size. These confined channels, which can be adjusted by nanosheet functionalization, are dominant in ion rejection. Meanwhile, different interactions among ions, water molecules, and functional groups of nanosheets further change the membrane water/salt selectivity. Therefore, through geometry and chemistry interaction with ions, GO membranes theoretically have great potential to achieve high water/salt selectivity for industrial water treatment applications.[8]

The effects of GO nanosheet functionalization are mainly dependent on their locations. A large number of functional groups are linked on the nanosheet surface. These surface functional groups can change the properties of interlayer channel surfaces and adjust the channel size. A higher nanosheet oxidation degree can enlarge the channel size as demonstrated by atomic force microscopy and transmission electron microscopy from experimental works at the micron scale.[9,10] At the edge of nanosheets, functional groups form the entrance of the interlayer channels and sieve ions out of water molecules after nanosheets are assembled.[11] Although a major factor in membrane desalination, edge functional groups are barely studied. Experimental investigation is quite limited due to their nanoscale size. Furthermore, the effects of different kinds of functional groups on desalination are very hard to identify because only the overall composition of functional groups on the nanosheets can be tested.[10,12] Therefore, numerical molecular dynamics (MD) simulations are utilized instead to zoom into the nanoscale membrane in order to study the effects of edge functional groups on desalination.

MD simulation has been widely used for elucidating the effects of surface functionalization in the layer-by-layer GO membranes.[10,13−17] The edge functional groups, whose sieving effect has been proposed to behave with the rejection effect in experimental works,[18,19] are rarely studied in simulation work.

Received: November 4, 2019
Accepted: December 30, 2019
Published: December 30, 2019

https://dx.doi.org/10.1021/acsami.9b19976
ACS Appl. Mater. Interfaces 2020, 12, 4769–4776

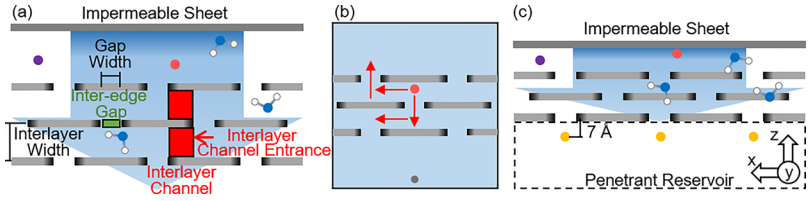

Figure 1. (a) Illustration of the layer-by-layer GO membrane structure for the overall water and ion transport performances. (b) Single-ion model inside the LP and HP membranes. The ion is represented with a red dot, the reference atom is represented with a gray dot, and the directions of restrained energy are represented with red arrows. (c) Pseudoequilibrium-charged model.

The comparison between different kinds of edge functional groups is hitherto only limited to water transport performance.[20,21] No work has ever compared their effects on desalination performance yet. Similar studies have been widely done on single-layer porous GO membranes, whose pore edges were functionalized by neutral or ionized carboxyl and hydroxyl[22−24] or were passivated with nitrogen,[23,25] hydrogen,[26−28] or fluorine[26,29] atoms through etching or guiding growth perforation.[30] When these functionalized groups are linked at the edges of 2D nanosheets, however, they control the intermembrane channels whose entering areas (Å × μm)[8] are much wider than the etched pores (nm × nm).[30] These edge functional groups influence the water permeance and ion rejection in absolutely different ways. Furthermore, the layer-by-layer membrane structure assembled by 2D nanosheets has better potential on large-scale preparation for commercial products with lower associated costs.[30] Therefore, to provide strategies for higher 2D-GO layer-by-layer membrane desalination efficiency, the study of ion rejection effects of edge functional groups on layer-by-layer GO membrane is necessary.

To address the gap in knowledge, three typical edge functional groups, which are carboxyl (COOH), hydroxyl (OH), and hydrogen (H),[7,31] were compared in this work. They were fully positioned at the edges of GO nanosheets. Three kinds of membrane structures mimicking different membrane porosities and interlayer channel sizes were used for investigating the influence of edge groups on the desalination performance. The first section of this work analyzes the overall NaCl rejection of these edge-functionalized membranes. The following section further investigates preferential ion rejection caused by the edge functional groups during the filtration process. In the new molecular insights gained from this study, the COOH edge rejected ions well, while OH and H edges had similar ion/water selectivity. The isolation effects of different kinds of edge functional groups of the GO nanosheets will help to develop high-efficiency GO membranes for saline water desalination.

METHODOLOGY

Nanosheet Structures. All-atom molecular structures of the edge-functionalized GO nanosheets were built by VEGA_ZZ 3.1.1. COOH groups, OH groups, or H atoms were linked at all-edge carbon atoms of a graphite nanosheet in random orientations and charged based on the Gasteiger method[32,33] (Figure S1). Although GO nanosheets are highly wavy in nature, in the nanometer scale that could be simulated with MD simulation, nanosheets are quite flat.[8] Therefore, the GO nanosheets used in this work were approximated as flat sheets for simplicity.

Membrane Filtration System. To elucidate the effects of the edge functional groups on ion sieving, the membrane gap width and interlayer distance were adjusted (Figure 1a). The gap width is defined as the distance between the closest atoms of two GO nanosheets in the same membrane layer. Gap widths of 7 and 14 Å were used here. When the gap width was set at 7 Å, there was one water layer in the inter-edge gap. Meanwhile, when the gap width was set at 14 Å, the tiniest interlayer channel was built and the entrance of the interlayer channel was trapped by the edge and surface of the nanosheets.[21] The interlayer widths are defined as the distance between two carbon atoms of two GO nanosheets in the adjacent membrane layers. Interlayer widths of 7 and 14 Å were also used here, inside which there were one and four water layers inside an interlayer channel, respectively.[21] [21] Moreover, it is noteworthy that 7 Å is smaller than the radius of the hydration shells of both Na^+ and Cl^-, which effectively forces the ions to dehydrate for transport inside the channels between the nanosheets (Figure S2).

Three membrane structures were used in this study: a low-porosity membrane with narrow interlayer channels (LP membrane, 7 Å gap width × 7 Å interlayer width shown in Figure S3a), high-porosity membrane with narrow interlayer channels (HP membrane, 14 Å gap width × 7 Å interlayer width, Figure S3b), and low-porosity membrane with wide interlayer channels (WLP membrane, 14 Å gap width × 7 Å interlayer width, Figure S3c). Duplicating and placing edge-functionalized nanosheets were according to the membrane structures. Two impermeable sheets were put on the top and bottom of the filtration facilities, which were initially over 80 and 20 Å away from the membranes, respectively. The space between them were filled with SPC (simple point charge) water molecules[34] (Figure S2f) for a water permeance test, and the feed solution was ionized with 0.45 mol/L NaCl for an ion rejection test.

Single-Ion Transport System. Eight edge-functionalized nanosheets were duplicated and placed as a filtration membrane according to the structure designed with narrow interlayer channels (Figure 1b). The box boundaries in the z direction were set over 50 Å away from the filtration facilities for system equilibrium. The box was filled with SPC water molecules. One Na^+ or Cl^- was positioned inside the membrane (locations are shown in Figure 1b with a red dot) and one fix neutral oxygen atom 18 Å below the membrane as a location reference for the single-ion transport analysis.

Pseudocharged System. To study the accumulation of unbalanced charge in the penetrant reservoir caused by different Na^+ and Cl^- transport speeds, the charge was positioned fixed in its penetrant reservoir beforehand to mimic the high-penetrant ion concentration. Two membrane configurations were selected for this part of the study: an HP-G-H membrane that had the most significant preferential Cl^- rejection and an LP-G-OH membrane that had the most significant preferential Na^+ rejection. A magnitude of ±9 e was

https://dx.doi.org/10.1021/acsami.9b19976
ACS Appl. Mater. Interfaces 2020, 12, 4769−4776

arbitrarily chosen to represent the selective ion accumulation. Each membrane exit was positioned with nine atoms (0.25 e each) in a row, and they were kept at a distance of 5 Å between each other (Figure S4). This charged ion row was fixed in the middle of the exit and 7 Å away from the membrane (Figure 1c). Throughout the simulation, the overall charge of the penetrant reservoir was continuously monitored to denote the ion permeability through the structured membranes.

Molecular Dynamics Simulation. All simulations were performed by large-scale atomic/molecular massively parallel simulator (LAMMPS) at a 2 fs time step under 300 K. The parameters of the Lennard-Jones (LJ) potential between GO membranes and water molecules were adapted from the parameters used by Chen et al.[35] and extended with Lorentz–Berthelot mixing rules[36] (Table S1). The cutoff radius of the LJ potential was set at 9 Å. The long-range electrostatic potential was calculated with the kspace_style PPPM solver. SPC water molecules were applied with the SHAKE algorithm.[34] Periodic boundary conditions were applied in all directions. The membrane area was extended in the x and y directions, while the box boundaries in the z direction were set 70 Å away from the filtration facility for system equilibrium.

Overall Permeance Analyses. The overall membrane performances of water and ion permeance were analyzed separately. The simulation was performed with *NVT*. Two impermeable sheets and all solution molecules were relaxed for system equilibrium for 40 ps. The top impermeable sheet was applied with a 5 kcal/(mol·Å) downward force every 10 steps to push the feed solution to go through the edge-functionalized membrane. Meanwhile, the bottom impermeable sheet was applied with a 0.01 kcal/(mol·Å) upward force every 10 steps to maintain the equilibrium state of the penetrant reservoir. Atom locations were recorded every 200 fs for analysis.

Water permeance is the water flux normalized with the transmembrane pressure and membrane area, which is

$$\text{water permeance} = \Delta m/(\Delta t \cdot S \cdot \Delta p)$$

where Δm is the mass of penetrant water molecules, Δt is the time of filtration, S is the membrane area, and Δp is the driving pressure. The driving pressure caused by the pressure difference between the feed and penetrant solution is calculated by a statistic equation

$$P = 113097\rho^3 - 290135\rho^2 + 262479\rho - 84744$$

where P (atm) is the hydraulic pressure and ρ (g/cm^3) is the water density.[21]

Ion rejection analyses were repeated three times for validation. The numbers of penetrant Na^+, Cl^-, and water molecules were started to be calculated when the first ion arrived in the penetrant reservoir. After 200 ps, the numbers were counted again, and the differences were calculated as the numbers of penetrant water molecules, Na^+, and Cl^-. Meanwhile, the number of ions was counted and averaged with a mesh size of 1 Å^3 to compute the ion retention time inside the membranes.

Single-Ion Transport Analyses. Single-ion transport analysis was designed for mapping the ion hydration degree and ion vibration. Metadynamics simulation in a harmonic biasing method with moving restraints[37] was undertaken with *NPT* at 1 atm. After equilibrium, the system for 2 ns, a moving window at 0.2 Å, and a moving speed at 1 Å/ns in the required direction were adopted for "collecting" the ion transport variables. Below are the methods used for calculating the coordination number of the ion hydration shells and the ion vibration velocity for analysis.

Ion Dehydration. Ion hydration sizes are defined as the oxygen shells around ions. The inner and outer hydration radii were 3.25 and 5.55 Å around Na^+ and 3.85 and 6.25 Å around Cl^-, respectively (Figure S2). During the transport process of a single ion, the coordination numbers of the hydration shells were collected and averaged to draw the ion hydration map inside membranes.

Ion Vibration Velocity. During the single-ion transport analyses, the ion moving velocity was calculated with the equation below:

$$v_i = \sqrt{(x_{i+t} - x_i)^2 + (y_{i+t} - y_i)^2 + (z_{i+t} - z_i)^2}/\Delta t$$

Collection and averaging of the moving speeds were performed at different locations inside the membranes to produce the ion vibration map discussed in the manuscript.

RESULTS AND DISCUSSION

Ion Rejection Performance. Comparing the significance of edge functional groups in different membrane channel sizes for identifying the influence of the membrane structure, when a membrane was assembled with wide interlayer channels, there was no difference between the three kinds of edge-functionalized membranes in terms of absolute or relative NaCl permeability (Figure 2i,l). When the size of the interlayer

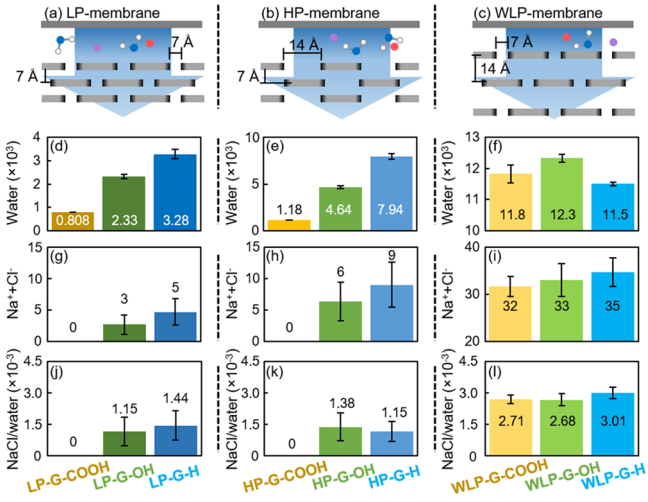

Figure 2. Three kinds of membrane configurations that have (a) low porosity and narrow interlayer channel, named the LP membrane, (b) high porosity and narrow interlayer channel, named the HP membrane, and (c) low porosity and wide interlayer channel, named the WLP membrane. Numbers of penetrant (d–f) water molecules and (g–i) NaCl and (j–l) the ratios of NaCl to water molecules when applied with hydraulic pressure. This part of the simulation was calculated with the Overall Permeance Analyses.

channel was decreased to 7 Å and the membrane became more compact, however, a significant effect caused by edge functional groups emerged regardless of the level of membrane porosity (Figure 2d,e,g,h,j,k). The LP and HP membranes had the same trend as water and NaCl permeance, which was G-COOH < G-OH < G-H (Figure 2d,e,g,h). Since the volumes of the membrane edges followed a trend of COOH edge > OH edge > H edge, it revealed that the geometric effect, which resulted in the steric blocking at the entrance of the interlayer

https://dx.doi.org/10.1021/acsami.9b19976
ACS Appl. Mater. Interfaces 2020, 12, 4769–4776

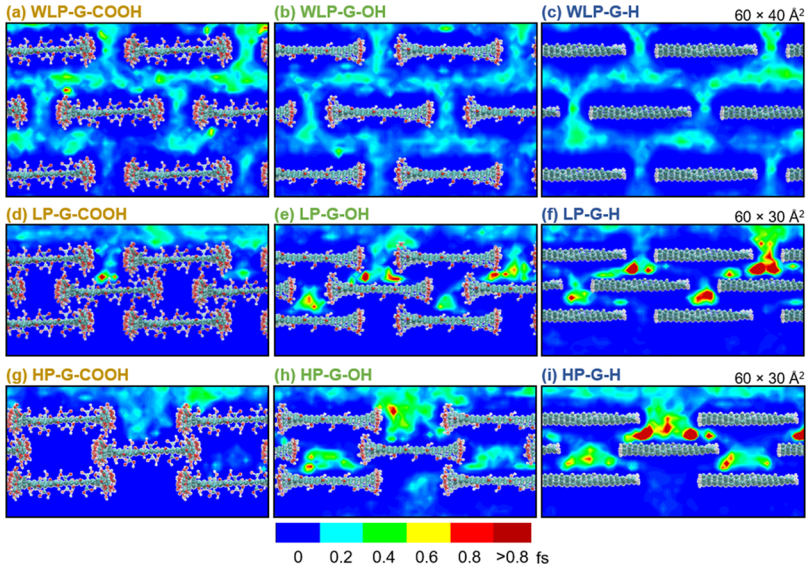

Figure 3. NaCl retention maps of the (a–c) WLP, (d–f) LP, and (g–i) HP membranes edge-functionalized by (a, d, g) COOH, (b, e, h) OH, and (c, f, i) H. Red areas represent the locations where ions stop for a long time, while the dark blue areas represent the locations where ions cannot reach or move fast.

channels, might be the dominant effect in ion rejection (the edge configurations are shown in Figure S1d–f, and the channel blockages, which had low water densities, are shown by the red arrows in Figure S5d,e,g,h).

If the geometric effect was the only effect that sieved larger hydrated NaCl from the small water molecules, higher NaCl/water selectivity was expected for the G-OH membrane. This was because the volume of the OH edge has a larger steric volume when compared to that of the H edge (Figure S1e,f). However, no significant difference was observed in the NaCl/water selectivity between the LP-G-OH, HP-G-OH, LP-G-H, or HP-G-H membranes (Figure 2j,k). The ion dehydration degree, which is the most commonly discussed aspect, cannot explain this phenomenon because Na^+ and Cl^- dehydration degrees inside two levels of membrane porosity were in conflict with each other (detailed analysis is discussed in the Supporting Information). Therefore, apart from the geometric sieving effect caused by different volumetric sizes of membrane edges, there must be some other factors at work in the ion rejection behavior observed that enhanced the salt permeance for the G-OH membranes.

One potential mechanism leading to ion selection might be ion adsorption, which referred to the mechanism that water permeance could be enhanced by stronger interaction between the water and nanosheet edges.[21] This type of stronger interaction helps water molecules to overcome the random molecular vibration and then be pulled into the narrow interlayer channels by the edge functional groups under the propelling mechanical hydraulic pressure (Figure 2f and Figure S3f). Similar hypothesis on ion selection was also revealed and proposed from reported experimental work.[6,38] We now attempt to discuss this possibility of quantitatively using the ion vibration parameter, which is a measure of the frequency of the Brownian motion of the ions.

Comparing the ion vibrations inside the membranes, the LP-G-COOH and HP-G-COOH membranes exhibited completely ion rejection (Figure 2j,k, and no ion trajectory could be observed inside the LP-G-COOH and HP-G-COOH membranes in Figure 3d,g). Significant lower vibrations for both Na^+ and Cl^- were observed inside both LP-G-OH and HP-G-OH membranes than those inside the G-H membranes (Figure 4a). In view of the fact that lower vibration could enhance water permeability, as discussed above, lower ion vibration caused by the OH edge could enhance the salt permeance to overcome the reduction in permeance caused by the volumetric blockage of the larger OH edge. This improvement of salt permeability was supported by the NaCl retention time comparison analysis as NaCl took more time to enter the LP-G-H and HP-G-H interlayer channels than to enter the G-OH ones (Figure 3e,f,h,i).

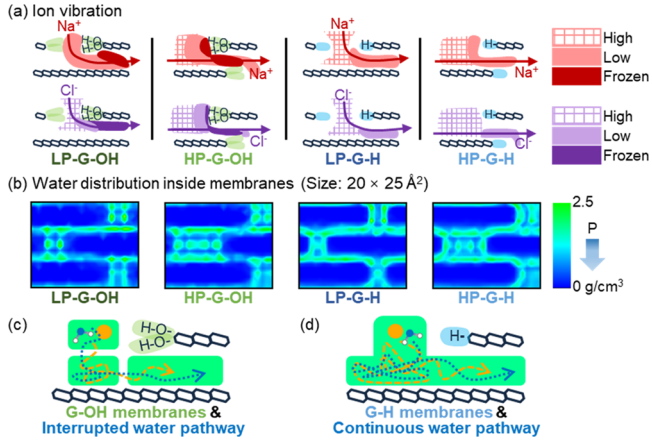

Figure 4. Filtration process inside the LP-G-OH, HP-G-OH, LP-G-H, and HP-G-H membranes. (a) Ion vibration in the equilibrium system while passing through the membrane channels filled with water molecules. This part was simulated with the Single-Ion Transport Analyses, and the original data is shown in Figure S6. (b) Water distribution inside the membranes when pure water was applied with hydraulic pressure. The dark blue area indicates the locations of the GO nanosheets or low water density, while the green area indicates the locations of high water density. The original data is shown in Figure S5. (c) Illustration of the interactional "ion pulling" effect of the G-OH membranes. (d) Illustration of the interactional "ion rejection" effect of the G-H membranes.

https://dx.doi.org/10.1021/acsami.9b19976
ACS Appl. Mater. Interfaces 2020, 12, 4769–4776

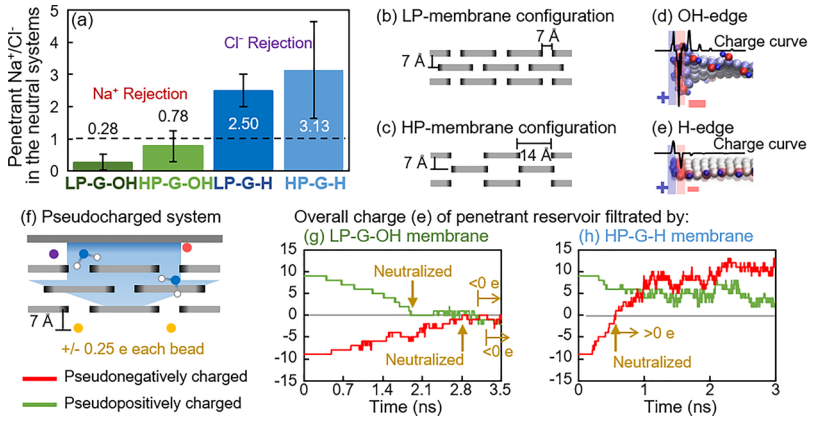

Figure 5. (a) Ratio of penetrant Na^+/Cl^- of the LP-G-OH, HP-G-OH, LP-G-H, and HP-G-H membranes. Illustration of the (b) LP and (c) HP membrane configurations. Illustration of the (d) OH and (e) H edges. The original data is shown in Figure S1. (f) Illustration of the pseudocharged model. Overall charge of the penetrant reservoirs of (g) LP-G-OH and (h) HP-G-H membrane pseudocharged filtration systems.

How does the OH edge decrease ion vibration and improve ion permeance? The first potential answer that comes to mind might be the direct interaction between the ion and nanosheet edge, which was proposed based on the water permeance enhancement mechanism[21] and the explanation commonly used for experimental results.[6,38] If the ion vibration was reduced by this interaction, the vibration inside the LP membranes should be reduced more because of their closer proximity between the edges of the nanosheets. The observation in Figure 4a, however, revealed otherwise. The overall vibration reduction nearby the functional groups was more significant in the HP membranes than in the LP membranes (Figure 4a), which means that the interaction between the ion and the edge is not the dominant effect in this case. Considering that the ions are surrounded by water molecules inside the membranes, their vibration may be affected also by the water molecules in their vicinity. This potential answer led us to further examine the water distribution within the membranes (Figure 4b and Figure S5). Inside the G-H membranes, water pathways were more continuous than those inside the G-OH membranes (Figure 4b, green areas show water pathways). The interrupted water pathway inside the G-OH membranes showed high attraction from the OH edges (Figure 4b). Following the guidance of the OH edge through interaction, water molecules therefore had little collision with ions. In an ordered transport manner, ions were easily pushed into the entrance of the interlayer channels and could achieve high permeability in the G-OH membranes (Figure 4c). Inside the G-H membranes, the continuous water pathway showed the poor attraction acted by the H edge and high vibration of water molecules (Figure 4b). Without edge guidance, both water molecules and ions moved in a disordered manner. The high collision between water molecules and ions largely reduced the ion permeability inside the G-H membranes (Figure 4d). Therefore, NaCl permeability was improved by the OH edge through a unique interactional "ion pulling" effect and reduced by the H edge through an interactional "ion rejection" effect.

A brief summary of the effect of edge functional groups on the NaCl permeance and NaCl/water selectivity is given as follows. The size of the edge functional groups determines the absolute NaCl penetrant number. Larger volumetric blockage caused by the edge functional groups reduces more NaCl permeance. Meanwhile, the edge functional groups influence the NaCl/water selectivity through guiding the movement of water molecules and reduce the collision between the water molecules and ions. Based on this mechanism, the OH edge reduced the NaCl/water selectivity to the same level as the H edge even though the OH edge was geometrically larger than the H edge.

Na^+ or Cl^- Rejection Preference. In addition to the ion permeance and NaCl/water selectivity behavior, an interesting phenomenon caused by the edge functional groups was also observed: the LP-G-OH and HP-G-OH membranes exhibited higher Na^+ rejection preference, while the LP-G-H and HP-G-H membranes behaved in an opposite manner with higher Cl^- rejection preference (Figure 5a and Figure S3g,h). Such Na^+/Cl^- selectivity, however, was not clearly observed under the wide conditions (Figure S3i). Similar differences in ion permeability between the cation and anion were also reported in other works.[24,39,40] Their differences, however, were not their main concerns[40] or were caused by the charged membranes for ionization.[24,39] In this study, however, the membranes were only neutrally edge-functionalized, which were different from ionized membranes. Therefore, the mechanism behind this special ion selectivity was quite intriguing.

The first possible reason for rejection preference could be the edge charge distribution, which has been used for explaining the ion selectivity of ionized membranes.[24,39] The OH and H edges, however, showed similar distribution in which their edges were both positively charged (Figure 5d,e and Figure S1e,f). Those positively charged edges ought to attract Cl^- and repulse Na^+ by electrostatic interaction, but two opposite preferential rejections were observed from the filtration results (Figure 5a). Thus, the ion transport behavior under the influence of the edge functional groups inside the membranes was compared to further unveil the underlying mechanism.

Examining the ion vibration map inside the membranes revealed that in addition to the lower vibration of both kinds of ions inside the G-OH membranes than that inside the G-H membranes (discussed in the previous section), Cl^- overall exhibited higher vibration than Na^+ (Figure 4a, the reason for this difference is discussed in the Supporting Information). With higher ion vibration, it is hard for Cl^- to enter the narrow interlayer channels compared to Na^+. This possibility was reduced more inside the G-H membranes because of a higher

https://dx.doi.org/10.1021/acsami.9b19976
ACS Appl. Mater. Interfaces 2020, 12, 4769−4776

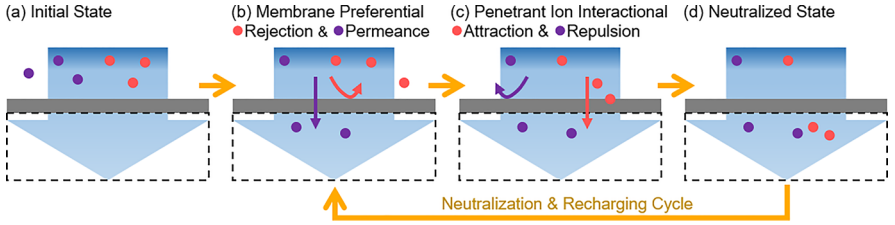

Figure 6. Illustration of the neutralization and recharging cycle of a preferential ion rejection membrane. Purple and red dots are reversely charged ions of each other.

collision between water molecules and ions caused by little attraction and guidance of the H edge (Figure 4d). Therefore, the LP-G-H and HP-G-H membranes showed the preferential Cl^- rejection.

Inside the LP-G-OH and HP-G-OH membranes, an opposite preferential ion rejection was observed (Figure 5a). The OH edge may reject ions with a different mechanism other than the H edge does. As discussed in the previous section, the ion vibrations were reduced by the ordered transported water molecules, which was caused by the interaction between water molecules and the OH edge. The differences between the two ions' vibrations may be negated inside the G-OH membranes. Accordingly, the interaction effect between the ions and the OH edge became more significant inside the G-OH membranes. The electrostatic repulsion acted by the positively charged H atoms of the OH edge rejected Na^+ and resulted in the preferential Na^+ rejection of the LP-G-OH and HP-G-OH membranes (Figure 5d). Higher ion selectivity of LP-G-OH than that of the HP-G-OH membrane further supported this hypothesis because the interaction effect became more noteworthy with the closer proximity between the edges of the nanosheets (Figure 5a). Consequently, the LP-G-H and HP-G-H membranes showed higher preferential Na^+ rejection for the vibration-pulling effect, while the LP-G-OH and HP-G-OH membranes showed higher preferential Cl^- rejection for the electrostatic interaction effect.

One question would be raised at this point: will this ion selectivity caused by the influence of edge functional groups be maintained at an extended filtration time? Continuing the preferential ion rejection, the charge would accumulate in the penetrant reservoir and may then promote the permeability of the counter ions. It might, in an overall manner, negate the membrane preferential ion selectivity. To ascertain this question, the ion filtration process of the HP-G-H (the most significant preferential Na^+ permeance) and the LP-G-OH (the most significant preferential Cl^- permeance) membranes with initially charged penetrant reservoirs was simulated for further study (Figure 5f).

By monitoring the overall charge of the penetrant reservoir at an extended filtration time, the negative overall charge, which was caused by the higher Cl^- permeance of the LP-G-OH membrane (Figure 5a), was still observed at the ends of both pseudopositively and pseudonegatively precharged models (Figure 5g). In the pseudonegative-charged system, an initially negatively charged penetrant reservoir increased the transport of Na^+ across the LP-G-OH membrane due to the electrostatic attraction. A progressive neutralization in the penetrant reservoir could be clearly observed (red line in Figure 5g). Once the penetrant reservoir charge approached the neutral state (at ~2.8 ns), the overall charge then hovered to be slightly negative even at an extended simulation time of 3.5 ns. This pseudonegative precharge is a clear sustained effect of the preferential Cl^- permeance of the LP-G-OH membrane. Conversely, an initially positive penetrant reservoir charge led to an even more preferential Cl^- permeance, allowing the penetrant reservoir to reach the neutral charge condition. After hovering around at the neutral charge condition for ~1.0 ns, the penetrant charge eventually became slightly negative at ~3.0 ns. Thus, the penetrant reservoir was always negatively charged regardless of the type of the initial penetrant reservoir charge, corresponding to the ion permeance characteristic of the LP-G-OH membrane as described in the neutral system (Figure 5a).

The HP-G-H membrane, which had significant preferential Na^+ permeance, showed similar behavior to the LP-G-OH membrane with a significantly positively charged penetrant reservoir at around +5 to +8 e (Figure 5h). In fact, for the pseudopositively precharged penetrant reservoir, the accelerated Cl^- permeance due to the attraction by the penetrant reservoir did not reduce the overall charge to neutral state prior to reaching the pseudo-equilibrium. For the pseudonegatively precharged penetrant reservoir, its charge reached the neutral state in a relatively faster manner (relative to the LP-G-OH case) before becoming positive in charge. These characteristics corresponded to the significantly higher preferential Na^+ permeance via the HP-G-H membrane.

Thus, the ion permeance selectivity was proven to be sustained as shown by the pseudocharged systems. Faster transported ion determined by the influence of edge functional groups charges the penetrant reservoir (from the state of Figure 6a,b) and exerts an electrostatic attraction on the feed reservoir, which improves the counter ions' permeance (Figure 6c). After subsequent neutralization, the electrostatic potential exerted by the penetrant reservoir becomes too weak to offset the ion transport differences (Figure 6d). Consequently, as the edge functional groups of the GO membranes determine the preferential ion rejection, this will lead to neutralization and recharging in a repeated cycle in the penetrant reservoir (Figure 6b–d).

CONCLUSIONS

In this work, the effects of COOH, OH, and H edge functionalization on NaCl rejection were investigated through MD simulation. Compared with the inter-edge gap, the membrane interlayer channel is the dominant location that reduces ion permeance. The effects of the three typical edge functional groups on both water permeance[21] and ion rejection are summarized in Figure 7. For an LP or HP membrane that has narrow interlayer channels, the COOH edge is recommended to induce high ion rejection because of its larger volumetric structure. If the GO membrane with high water permeability and ion rejection must be prepared, the H edge is recommended because it is smaller and it can reject ion

https://dx.doi.org/10.1021/acsami.9b19976
ACS Appl. Mater. Interfaces 2020, 12, 4769–4776

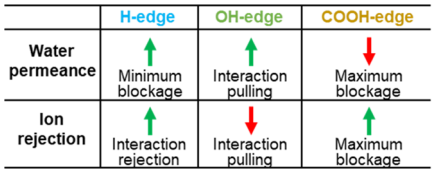

Figure 7. Summarized effects of edge functional groups on water permeance[21] and ion rejection.

through the interactional ion rejection effect. Furthermore, because the overall NaCl/water selectivity of the LP-G-OH, HP-G-OH, LP-G-H, and HP-G-H membranes are very similar, the structure that has higher membrane porosity is also recommended.

Another interesting phenomenon observed in this work was the effect of the edge functional groups on preferential ion rejection. This difference between Na^+ and Cl^- permeabilities will lead to a repeated cycle of charging and neutralizing the penetrant reservoir. Therefore, membrane charges up may be strategic to improve membrane desalination performance. This desalination work in simulation shows great potential of a numerical method for the separation study of larger ions and small organic ions, which may achieve high ion selectivity by the 2D GO membranes for their special complex configurations and interactions.

■ ASSOCIATED CONTENT

Supporting Information

The Supporting Information is available free of charge at https://pubs.acs.org/doi/10.1021/acsami.9b19976.

Original data of analysis, discussion on ion dehydration, and reason for different ion vibration degrees (PDF)

■ AUTHOR INFORMATION

Corresponding Author

Meng Wai Woo − *Monash University, Clayton, Australia, and The University of Auckland, Auckland, New Zealand;* orcid.org/0000-0002-3268-8191; Email: meng.woo@monash.edu

Other Authors

Ruosang Qiu − *Monash University, Clayton, Australia;* orcid.org/0000-0001-6086-1935

Jie Xiao − *Soochow University, Suzhou, PR China;* orcid.org/0000-0001-7842-7862

Xiao Dong Chen − *Soochow University, Suzhou, PR China*

Cordelia Selomulya − *Monash University, Clayton, Australia, and UNSW, Sydney, Australia*

Xiwang Zhang − *Monash University, Clayton, Australia;* orcid.org/0000-0002-4319-527X

Complete contact information is available at: https://pubs.acs.org/10.1021/acsami.9b19976

Author Contributions

The manuscript was written through contributions of all authors. All authors have given approval to the final version of the manuscript.

Funding

This project was supported by the Australian Government Department of Industry, Innovation, and Science through the Australia-China Science and Research Fund (ACSRF48154) and the National Key Research and Development Program of China (International S&T Cooperation Program, ISTCP, 2016YFE0101200).

Notes

The authors declare no competing financial interest.

■ ACKNOWLEDGMENTS

This project was supported by the Australian Government Department of Industry, Innovation, and Science through the Australia−China Science and Research Fund (ACSRF48154) and was conducted as part of the research program of the Australia−China Joint Research Centre in Future Dairy Manufacturing (http://acjrc.eng.monash.edu/). Soochow University acknowledges The National Key Research and Development Program of China (International S&T Cooperation Program, ISTCP, 2016YFE0101200) for support of the Australia−China collaboration.

■ ABBREVIATIONS

GO, graphene oxide
G, graphene
COOH, carboxyl
OH, hydroxyl
H, hydrogen
2D, two-dimensional
MD, molecular dynamics
LP, low membrane porosity with narrow interlayer channels
HP, high membrane porosity with narrow interlayer channels
WLP, low membrane porosity with wide interlayer channels
SPC, simple point charge
W, water
LJ potential, Lennard-Jones potential

■ REFERENCES

(1) Shiklomanov, I. A.; Rodda, J. C. Eds. *World Water Resources at the Beginning of The Twenty-First Century*; Cambridge University Press, 2004.

(2) Elimelech, M.; Phillip, W. A. The Future of Seawater Desalination: Energy, Technology, and The Environment. *Science* **2011**, *333*, 712−717.

(3) Voutchkov, N. Energy Use for Membrane Seawater Desalination−Current Status and Trends. *Desalination* **2018**, *431*, 2−14.

(4) Yan, F.; Chen, H.; Lü, Y.; Lü, Z.; Yu, S.; Liu, M.; Gao, C. Improving The Water Permeability and Antifouling Property of Thin-Film Composite Polyamide Nanofiltration Membrane by Modifying The Active Layer with Triethanolamine. *J. Membr. Sci.* **2016**, *513*, 108−116.

(5) Soice, N. P.; Maladono, A. C.; Takigawa, D. Y.; Norman, A. D.; Krantz, W. B.; Greenberg, A. R. Oxidative Degradation of Polyamide Reverse Osmosis Membranes: Studies of Molecular Model Compounds and Selected Membranes. *J. Appl. Polym. Sci.* **2003**, *90*, 1173−1184.

(6) Epsztein, R.; Shaulsky, E.; Qin, M.; Elimelech, M. Activation Behavior for Ion Permeation in Ion-exchange Membranes: Role of Ion Dehydration in Selective Transport. *J. Membr. Sci.* **2019**, *580*, 316−326.

(7) Dreyer, D. R.; Park, S.; Bielawski, C. W.; Ruoff, R. S. The Chemistry of Graphene Oxide. *Chem. Soc. Rev.* **2010**, *39*, 228−240.

(8) Kang, Y.; Xia, Y.; Wang, H.; Zhang, X. 2D Laminar Membranes for Selective Water and Ion Transport. *Adv. Funct. Mater.* **2019**, *29*, 1902014.
(9) Balapanuru, J.; Manga, K. K.; Fu, W.; Abdelwahab, I.; Zhou, G.; Li, M.; Lu, H.; Loh, K. P. Desalination Properties of A Free-Standing, Partially Oxidized Few-Layer Graphene Membrane. *Desalination* **2019**, *451*, 72−80.
(10) Zheng, S.; Tu, Q.; Urban, J. J.; Li, S.; Mi, B. Swelling of Graphene Oxide Membranes in Aqueous Solution: Characterization of Interlayer Spacing and Insight into Water Transport Mechanisms. *ACS Nano* **2017**, *11*, 6440−6450.
(11) Liu, J.; Yu, L.-J.; Yue, G.; Wang, N.; Cui, Z.; Hou, L.; Li, J.; Li, Q.; Karton, A.; Cheng, Q.; Jiang, L.; Zhao, Y. Thermoresponsive Graphene Membranes with Reversible Gating Regularity for Smart Fluid Control. *Adv. Funct. Mater.* **2019**, *29*, 1808501.
(12) Xia, S.; Ni, M.; Zhu, T.; Zhao, Y.; Li, N. Ultrathin Graphene Oxide Nanosheet Membranes with Various D-Spacing Assembled Using The Pressure-assisted Filtration Method for Removing Natural Organic Matter. *Desalination* **2015**, *371*, 78−87.
(13) Ayappa, K. G.; Rajasekaran, M. Enhancing the Dynamics of Water Confined between Graphene Oxide Surfaces with Janus Interfaces: A Molecular Dynamics Study. *J. Phys. Chem. B* **2019**, *123*, 2978−2993.
(14) Wang, F.; You, Y.; Jin, X.; Joshi, R. On the Role of Driving Force in Water Transport through Nanochannels within Graphene Oxide Laminates. *Nanoscale* **2018**, *10*, 21625−21628.
(15) Chen, B.; Jiang, H.; Liu, X.; Hu, X. Observation and Analysis of Water Transport through Graphene Oxide Interlamination. *J. Phys. Chem. C* **2017**, *121*, 1321−1328.
(16) Willcox, J. A. L.; Kim, H. J. Molecular Dynamics Study of Water Flow across Multiple Layers of Pristine, Oxidized, and Mixed Regions of Graphene Oxide: Effect of Graphene Oxide Layer-to-Layer Distance. *J. Phys. Chem. C* **2017**, *121*, 23659−23668.
(17) Li, W.; Zheng, X.; Dong, Z.; Li, C.; Wang, W.; Yan, Y.; Zhang, J. Molecular Dynamics Simulations of CO_2/N_2 Separation through Two-Dimensional Graphene Oxide Membranes. *J. Phys. Chem. C* **2016**, *120*, 26061−26066.
(18) Huang, H.; Song, Z.; Wei, N.; Shi, L.; Mao, Y.; Ying, Y.; Sun, L.; Xu, Z.; Peng, X. Ultrafast Viscous Water Flow through Nanostrand-channelled Graphene Oxide Membranes. *Nat. Commun.* **2013**, *4*, 2979.
(19) Nair, R. R.; Wu, H. A.; Jayaram, P. N.; Grigorieva, I. V.; Geim, A. K. Unimpeded Permeation of Water through Helium-leak−tight Graphene-based Membranes. *Science* **2012**, *335*, 442−444.
(20) Safaei, S.; Tavakoli, R. On the Design of Graphene Oxide Nanosheets Membranes for Water Desalination. *Desalination* **2017**, *422*, 83−90.
(21) Qiu, R.; Yuan, S.; Xiao, J.; Chen, X. D.; Selomulya, C.; Zhang, X.; Woo, M. W. Effects of Edge Functional Groups on Water Transport in Graphene Oxide Membranes. *ACS Appl. Mater. Interfaces* **2019**, *11*, 8483−8491.
(22) Cohen-Tanugi, D.; Grossman, J. C. Water Desalination across Nanoporous Graphene. *Nano Lett.* **2012**, *12*, 3602−3608.
(23) Li, Y.; Xu, Z.; Liu, S.; Zhang, J.; Yang, X. Molecular Simulation of Reverse Osmosis for Heavy Metal Ions Using Functionalized Nanoporous Graphenes. *Comput. Mater. Sci.* **2017**, *139*, 65−74.
(24) Konatham, D.; Yu, J.; Ho, T. A.; Striolo, A. Simulation Insights for Graphene-based Water Desalination Membranes. *Langmuir* **2013**, *29*, 11884−11897.
(25) Riyaz, M.; Goel, N. A QM/MM Study to Investigate Selectivity of Nanoporous Graphene Membrane for Arsenate and Chromate Removal from Water. *Chem. Phys. Lett.* **2017**, *685*, 371−376.
(26) Azamat, J. Functionalized Graphene Nanosheet as A Membrane for Water Desalination Using Applied Electric Fields: Insights from Molecular Dynamics Simulations. *J. Phys. Chem. C* **2016**, *120*, 23883−23891.
(27) Wang, Y.; He, Z.; Gupta, K. M.; Shi, Q.; Lu, R. Molecular Dynamics Study on Water Desalination through Functionalized Nanoporous Graphene. *Carbon* **2017**, *116*, 120−127.
(28) Zhang, L.; Wu, C.; Fang, Y.; Ding, X.; Sun, J. Computational Design of Porous Graphenes for Alkane Isomer separation. *J. Phys. Chem. C* **2017**, *121*, 10063−10070.
(29) Azamat, J.; Khataee, A.; Joo, S. W. Molecular Dynamics Simulation of Trihalomethanes Separation from Water by Functionalized Nanoporous Graphene under Induced Pressure. *Chem. Eng. Sci.* **2015**, *127*, 285−292.
(30) Guirguis, A.; Maina, J. W.; Kong, L.; Henderson, L. C.; Rana, A.; Li, L. H.; Majumder, M.; Dumée, L. F. Perforation Routes Towards Practical Nano-porous Graphene and Analogous Materials Engineering. *Carbon* **2019**, *155*, 660−673.
(31) Lerf, A.; He, H.; Forster, M.; Klinowski, J. Structure of Graphite Oxide Revisited. *J. Phys. Chem. B* **1998**, *102*, 4477−4482.
(32) Marsili, M.; Gasteiger, J. π Charge Distribution from Molecular Topology and π Orbital Electronegativity. *Croat. Chem. Acta* **1980**, *53*, 601−614.
(33) Gasteiger, J.; Marsili, M. Iterative Partial Equalization of Orbital Electronegativity- A Rapid access to Atomic Charges. *Tetrahedron* **1980**, *36*, 3219−3228.
(34) Mark, P.; Nilsson, L. Structure and Dynamics of the TIP3P, SPC, and SPC/E Water Models at 298 K. *J. Phys. Chem. A* **2001**, *105*, 9954−9960.
(35) Chen, B.; Jiang, H.; Liu, X.; Hu, X. Molecular Insight into Water Desalination across Multilayer Graphene Oxide Membranes. *ACS Appl. Mater. Interfaces* **2017**, *9*, 22826−22836.
(36) Xu, W.; Lan, Z.; Peng, B. L.; Wen, R. F.; Ma, X. H. Effect of Surface Free Energies on The Heterogeneous Nucleation of Water Droplet: A Molecular Dynamics Simulation Approach. *J. Chem. Phys.* **2015**, *142*, No. 054701.
(37) Fiorin, G.; Klein, M. L.; Hénin, J. Using Collective Variables to Drive Molecular Dynamics Simulations. *Mol. Phys.* **2013**, *111*, 3345−3362.
(38) Wang, M.; Shen, W.; Ding, S.; Wang, X.; Wang, Z.; Wang, Y.; Liu, F. A Coupled Effect of Dehydration and Electrostatic Interactions on Selective Ion Transport through Charged Nanochannels. *Nanoscale* **2018**, *10*, 18821−18828.
(39) Fang, C.; Yu, Z.; Qiao, R. Impact of Surface Ionization on Water Transport and Salt Leakage through Graphene Oxide Membranes. *J. Phys. Chem. C* **2017**, *121*, 13412−13420.
(40) Gogoi, A.; Konch, T. J.; Raidongia, K.; Reddy, K. A. Water and Salt Dynamics in Multilayer Graphene Oxide (GO) Membrane: Role of Lateral Sheet Dimensions. *J. Membr. Sci.* **2018**, *563*, 785−793.

https://dx.doi.org/10.1021/acsami.9b19976
ACS Appl. Mater. Interfaces 2020, 12, 4769−4776